New Mexico Geological Society

Downloaded from: https://nmgs.nmt.edu/publications/guidebooks/71



Horizontal shortening of the Laramide Zuni Arch, west-central New Mexico: A preliminary study

Jacob O. Thacker
2021, pp. 281-290. https://doi.org/10.56577/FFC-71.281

in:

Geology of the Mount Taylor area, Frey, Bonnie A.; Kelley, Shari A.; Zeigler, Kate E.; McLemore, Virginia T.; Goff, Fraser; Ulmer-Scholle, Dana S., New Mexico Geological Society 71st Annual Fall Field Conference Guidebook, 310 p. https://doi.org/10.56577/FFC-71

This is one of many related papers that were included in the 2021 NMGS Fall Field Conference Guidebook.

Annual NMGS Fall Field Conference Guidebooks

Every fall since 1950, the New Mexico Geological Society (NMGS) has held an annual Fall Field Conference that explores some region of New Mexico (or surrounding states). Always well attended, these conferences provide a guidebook to participants. Besides detailed road logs, the guidebooks contain many well written, edited, and peer-reviewed geoscience papers. These books have set the national standard for geologic guidebooks and are an essential geologic reference for anyone working in or around New Mexico.

Free Downloads

NMGS has decided to make peer-reviewed papers from our Fall Field Conference guidebooks available for free download. This is in keeping with our mission of promoting interest, research, and cooperation regarding geology in New Mexico. However, guidebook sales represent a significant proportion of our operating budget. Therefore, only *research papers* are available for download. *Road logs*, *mini-papers*, and other selected content are available only in print for recent guidebooks.

Copyright Information

Publications of the New Mexico Geological Society, printed and electronic, are protected by the copyright laws of the United States. No material from the NMGS website, or printed and electronic publications, may be reprinted or redistributed without NMGS permission. Contact us for permission to reprint portions of any of our publications.

One printed copy of any materials from the NMGS website or our print and electronic publications may be made for individual use without our permission. Teachers and students may make unlimited copies for educational use. Any other use of these materials requires explicit permission.

This page is intentionally left blank to maintain order of facing pages.

New Mexico Geological Society Guidebook, 71st Field Conference, Geology of the Mount Taylor Area, 2021, p. 281-289.

HORIZONTAL SHORTENING OF THE LARAMIDE ZUNI ARCH, WEST-CENTRAL NEW MEXICO: A PRELIMINARY STUDY

Jacob O. Thacker

New Mexico Bureau of Geology and Mineral Resources, 801 Leroy Place, Socorro, NM 87801; jacob.thacker@nmt.edu

Abstract—The Zuni Mountains are an anticlinal Laramide arch with marked asymmetry along its southwestern forelimb (Nutria monocline), a low-elevation basement-involved range crest, and a gentle northeast-dipping backlimb (Chaco Slope). However, the range exhibits considerable along-strike complexity at odds with this simplistic framework. In the northwest Zuni arch, folds are southwest vergent, and the two dominant reverse faults, the Stinking Springs and McGaffey faults, strike north to northwest and exhibit east to northeast dips. In the southeast Zuni arch, the dominant fold pattern is northeast vergent and the Sedgwick reverse fault is largely north-northwest striking and exhibits a west to southwest dip. Minor fault data (strike-slip, conjugate strike-slip, and thrust) from these northwest and southeast domains show that early horizontal shortening preceded significant folding and faulting, as suggested by restoring bedding to horizontal, and both domains share similar geometric and kinematic results despite opposing fault polarities and variably-striking (i.e., E-W or N-S) beds from which minor faults are documented. Similarly, both domains and the range record WSW-ENE directed shortening (051–073° azimuth; 061° mean azimuth) that is consistent with estimates of shortening on numerous other Laramide arches in the Colorado Plateau and Rocky Mountains. Comparable shortening azimuths suggest that deformational processes between the Colorado Plateau and Rocky Mountain regions during the Late Cretaceous–Paleogene were similar, and therefore ENE horizontal shortening is the likely means by which the Zuni arch deformed during Laramide orogenesis. These results and interpretations are not in accord with previously suggested models for Zuni arch formation by mass transfer and/or Eurasian-style extrusion tectonics.

INTRODUCTION

The Zuni Mountains (Fig. 1), located between Gallup, Ramah, and Grants, New Mexico, are a structural arch (the "Zuni arch") that formed during the Cretaceous–Paleogene Laramide orogeny (Kelley, 1967). The range is in part a reactivated portion of the earlier and likely larger Zuni-Defiance uplift that formed during the Pennsylvanian–Permian Ancestral Rocky Mountains orogeny (Ross and Ross, 1986). Although the Zuni arch comprises one of the classic Laramide structures of the Colorado Plateau, its deformation history and structural characteristics have received comparatively little attention. Complex deformation is observed throughout the range in the form of (1) opposing reverse fault polarities at either end of the range, (2) a sinuous range crest, and (3) numerous faults of variable orientation. The preliminary dataset presented herein seeks to address some of this complexity by analyzing the geometry and kinematics of a handful of minor faults in post-Pennsylvanian (post-Ancestral Rocky Mountains) rocks across the Zuni Mountains. Many fault kinematic studies have been conducted in both the Colorado Plateau (e.g., Bump and Davis, 2003; Bump, 2004) and the Rocky Mountains (e.g., Erslev and Koenig, 2009; Weil and Yonkee, 2012; Singleton et al., 2019) and provide a base by which to analyze the Zuni arch with similar methods and to compare the results with a regional dataset. Such work has implications for Laramide deformation on the Colorado Plateau, the connection (in space, time, and style) of Colorado Plateau Laramide arches to their larger Rocky Mountain counterparts, and, overall, the tectonic processes responsible for intracontinental strain that formed Laramide arches of the interior western United States.

Past studies on the Zuni arch have evoked markedly different interpretations than those presented in this paper, warranting future research on the range. For example, Anderson et al. (2003) suggested initial vertical uplift via mid- to lower-crustal mass transfer followed by later horizontal shortening for the northwestern Zuni Mountains, an idea that is tested in this paper through structural analysis. Additionally, Chamberlin and Anderson (1989) also utilized fault slickenline data at a number of locations around the range to suggest that the Zuni Mountains formed by Eurasian style extrusion tectonics related to a rigid mid-crustal mafic anomaly south of the south-central Zuni arch. Chamberlin and Anderson (1989) postulated that this mafic "indenter" pushed the southeast Zuni Mountains up north/northeastward and laterally extruded the northwest Zuni Mountains westward, as expressed through numerous strike-slip and reverse faults within the range. This kinematic model is tested in this paper. Mafic crustal anomalies are of interest in other parts of the Laramide foreland (e.g., Bighorn arch, Wyoming: Worthington et al., 2016), and their role in localizing upper crustal strain warrants consideration. This paper builds on these previous works with an expanded dataset on a diverse array of fault types in different parts of the range and comes to a different conclusion for the tectonic processes that formed the Zuni arch.

In short, two objectives are addressed in this paper:

1. What is the structural framework of the Zuni Mountains (fault geometries and kinematics), and what might be the cause of structural complexity observed?
2. What was the shortening direction responsible for deformation? Is it consistent at each end of the range? How does it compare to other Laramide arches and what does it imply for the tectonic processes that drove deformation?

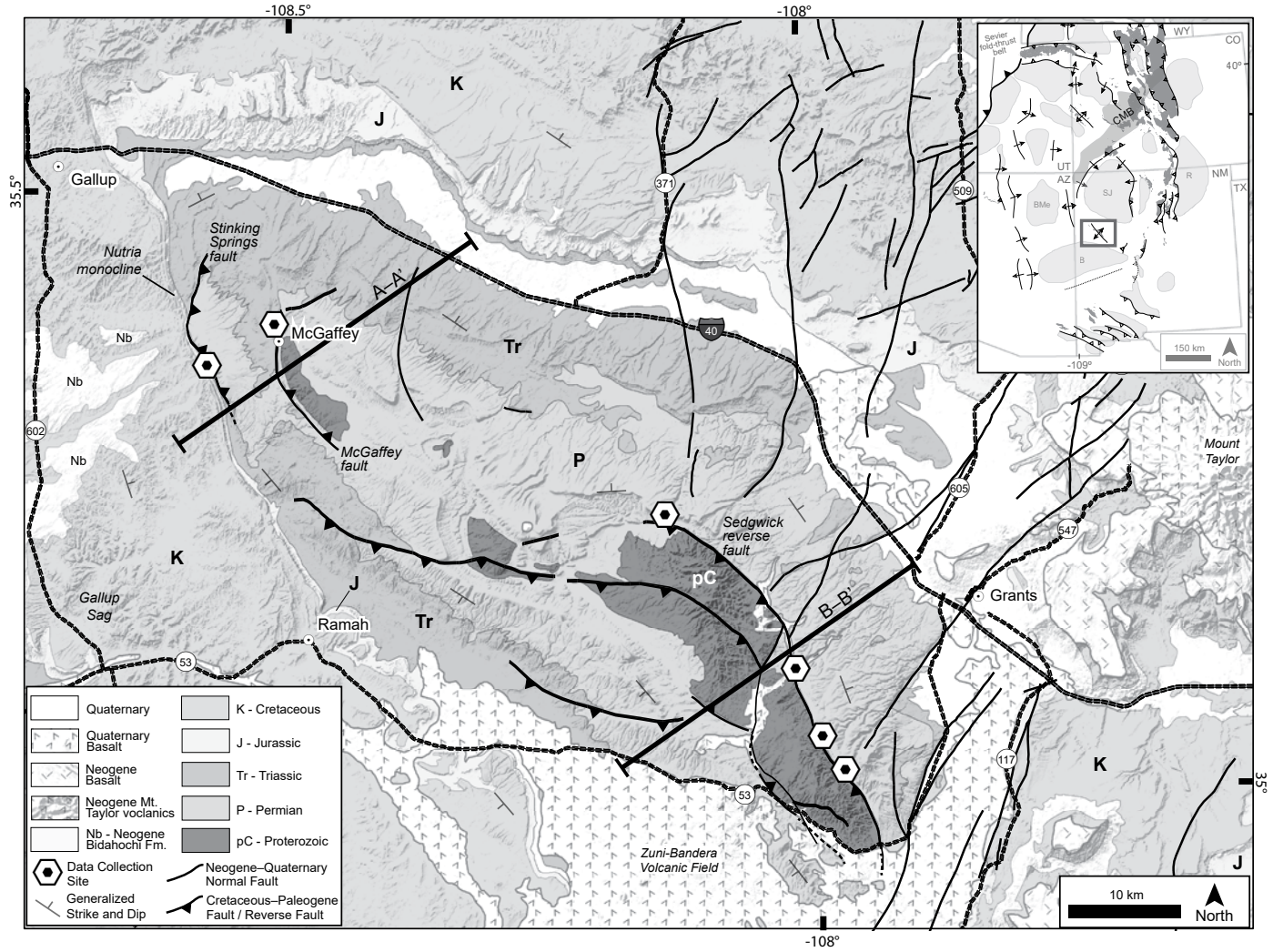


FIGURE 1. Simplified geologic map of the Zuni Mountains showing cross section locations (Fig. 2) and data collection sites. Inset map shows relative position of the Zuni arch in the southern Laramide foreland region. B – Baca basin; BMe – Black Mesa basin; R – Raton Basin; SJ – San Juan Basin; CMB – Colorado Mineral Belt. Geologic map data modified from Green and Jones (1997).

To address these questions, preliminary geometric and kinematic data and paleostrain analyses are presented in order to characterize fault geometries and to infer the orientation of Laramide shortening. Zuni arch data show characteristic fault geometries and a mean shortening azimuth of 061°. The estimated shortening direction is consistent with other Laramide arches across the Colorado Plateau and Rocky Mountain regions from Montana–South Dakota to Arizona–New Mexico, and suggests of a common deformational process that was pervasive throughout the entire Laramide foreland. Lastly, the structural data is used to address some of the complex deformation exhibited by the Zuni arch, namely opposing reverse fault polarities at each end of the range. It is hypothesized that a zone of sinistral displacement transfer accommodated strain between these two opposing domains (northwest and southeast), although there are currently insufficient data to fully make this claim. Future work will help to test this hypothesis, as well as other unanswered structural questions related to the Zuni arch.

GEOLOGIC SETTING AND LARAMIDE STRUCTURAL FRAMEWORK

The Zuni Mountains are situated on the southeastern Colorado Plateau and form the southwestern margin of the San Juan Basin, the northern margin of the Baca basin, and the eastern margin of the Gallup sag (Fig. 1; Cather, 2004). Proterozoic basement rock is exposed at four localities and, within the southeastern Zuni Mountains, is dated at ca. 1630 and ca. 1430 Ma (Strickland et al., 2003). Basement rock in the region was uplifted and exposed during the Pennsylvanian–Permian Ancestral Rocky Mountains orogeny as part of the larger Zuni-Defiance Uplift (Ross and Ross, 1986) and was subsequently buried by late Paleozoic through Mesozoic sedimentation. Western Interior Cretaceous Seaway sedimentation started with deposition of the Upper Cretaceous Dakota Sandstone. Structural partitioning of the San Juan Basin took place in the Late Cretaceous–Paleogene Laramide orogeny and resulted in a change to localized Paleocene–Eocene basin-fill sedimentation (Cather, 2004).

Commonly considered to be the result of flat slab subduction of the Farallon plate (Coney and Reynolds, 1977; Dickinson and Snyder, 1978), the Laramide orogeny was responsible for the formation of large basement involved ("thick skinned") arches and deep intermontane basins throughout the interior western United States, as presently exposed from Montana–South Dakota to southern Arizona–New Mexico. In west-central New Mexico, Laramide deformation may have commenced ca. 80–75 Ma, based on northeast-directed paleoflow indicators that suggest a paleohighland developing in the vicinity of the Defiance Mountains (Arizona–New Mexico state line) and Zuni Mountains (Cather, 2004). Inversely modeled apatite fission-track and apatite (U-Th)/He thermochronology data similarly suggest deformation of the Zuni arch commenced ca. 84–77 Ma (Thacker et al., unpubl. data).

Structurally, the Zuni arch encompasses a greater area than the present physiographic expression of the Zuni Mountains. The arch forms an overall NW-SE–striking, basement-involved, doubly plunging anticline with sharp forelimb asymmetry to the southwest along the Nutria monocline (Figs. 1, 2A; Darton, 1928; Edmonds, 1961) and a gentle northeast-dipping backlimb (Chaco Slope). The Zuni range crest is sinuous, and trends northwesterly in the northwest, easterly in the central part of the range, and again northwesterly in the southeast part of the range (Fig. 1). Although the overall structure is that of a southwest-facing asymmetric arch, the Zuni Mountains display marked along-strike complexity. Range-scale cross sections (Figs. 2A, B) and the simplified geologic map (Fig. 1) display a clear change in reverse fault polarity and fold vergence from the northwestern to southeastern Zuni arch. In the northwest, northeast-dipping reverse faults at the range front and near the town of McGaffey, New Mexico (Stinking Springs and McGaffey faults, respectively) create a southwest-facing asymmetric anticline with a more gently dipping backlimb (Fig. 2A). In the southeast, asymmetry is to the northeast via the southwest-dipping Sedgwick reverse fault (Fig. 2B; as shown by Goddard, 1966 and Timmons and Cikoski, 2012), although smaller-scale northeast-dipping reverse faults core southwest-vergent folds on the southwest side of the range here (Figs. 1, 2B). The central Zuni arch is characterized by easterly-striking faults, consistent with the easterly-trending range crest (Fig. 1). Numerous faults and folds are present (e.g., Hackman and Olson, 1977) that are attributable to Laramide deformation and make for a dense and complex array of faults throughout the range.

Late Cenozoic normal faults are evident in the study area, dominantly on the eastern part of Zuni arch (Fig. 1). These faults may represent the western extreme of the Rio Grande rift, Jemez Lineament volcanism and/or igneous intrusions, or some combination of each, but the structures are more likely reactivated Laramide faults related to the northern Hickman fault zone (Cather, 1990). Normal faults are approximately N-S to NNE-SSW striking. Extensional faults have not significantly affected the range, though notable exceptions do occur (e.g., near Zuni Canyon; Fig. 2B). Faults in the southeastern part of the range are coincident with Cenozoic basalt flows and cinder cone volcanoes of the Zuni-Bandera volcanic field.

METHODS

Geometric and kinematic structural data were collected dominantly from brittle minor faults (strike-slip, conjugate strike-slip, and thrust) and fractures in Permian Abo Formation through Upper Cretaceous Gallup Sandstone in the northwest-

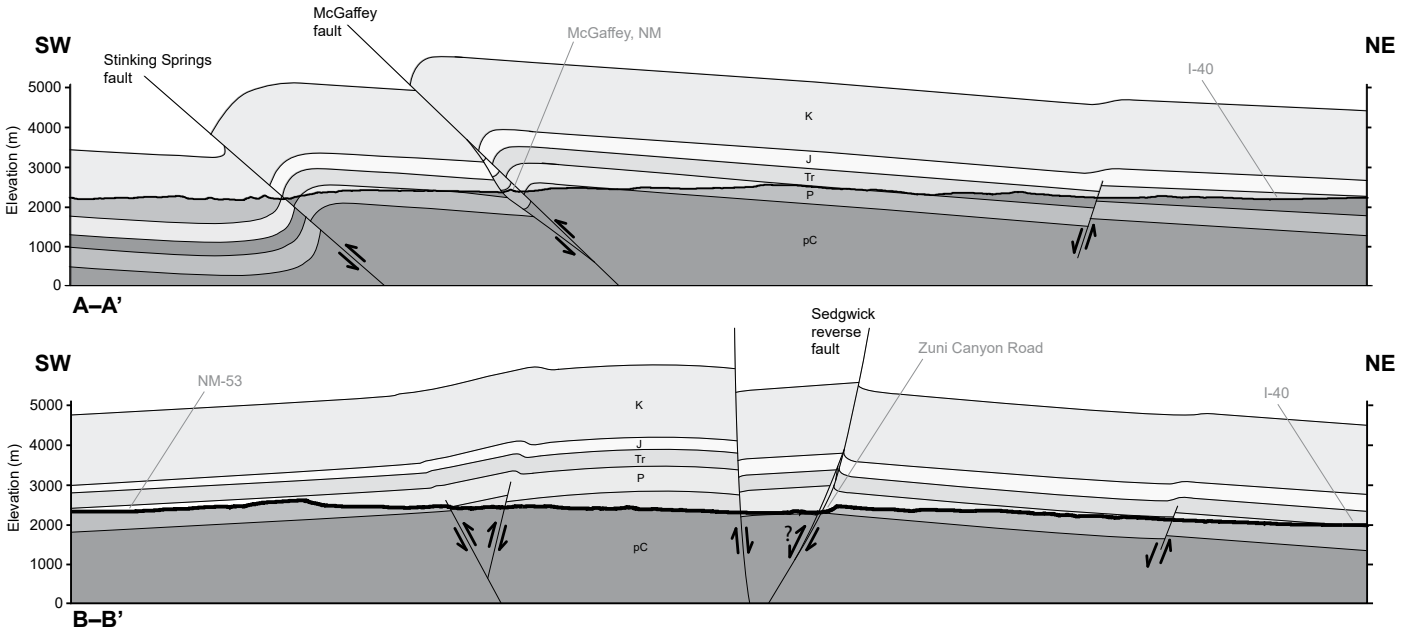


FIGURE 2. Admissible range-scale cross sections (locations shown in Fig. 1) of the Zuni Mountains (no vertical exaggeration). **A**) Northwest Zuni Mountains. Note range asymmetry to southwest. **B**) Southeast Zuni Mountains. Note complexity in deformation compared to northwest Zuni Mountains and change in dominate thrust polarity along the Sedgwick reverse fault.

ern and southeastern parts of the range (Fig. 1). Most minor fault data were collected near map-scale faults (Fig. 1). Pennsylvanian (and possibly older) units were largely stripped from the range during the Ancestral Rocky Mountains orogeny; minor faults in Pennsylvanian units are exposed in select localities throughout the range (Bursum Formation; Timmons and Cikoski, 2012) but were excluded to avoid collecting data from faults that formed during this earlier contractional episode. All post-Pennsylvanian minor faults were considered to have formed during the Late Cretaceous because of a lack of contractional tectonism for the region between the late Permian–Early Cretaceous. Bedding orientations were measured at every data collection site for retrodeformation of minor fault data and ranged between 15°–68° dip and N-S to E-W strike. Minor fault slip sense was determined using kinematic criteria outlined by Petit (1987) or through observable outcrop displacements (Fig. 3). In many instances, conjugate fault and fracture sets were observed that lacked slip-sense criteria, although their relative slip sense could be assumed based on their geometry (e.g., conjugate) and/or nearby conjugate faults of comparable orientation that exhibited positively identifiable slip-sense criteria.

The programs Stereonet (Allmendinger et al., 2012; Cardozo and Allmendinger, 2013) and FaultKin (Marrett and Allmendinger, 1990; Allmendinger et al., 2012) were used to process and analyze structural data. For geometric data (Fig. 3), Stereonet was used to calculate a cylindrical best fit from poles to planes in order to determine statistically significant populations and mean planes from eigenvalue statistics (Vollmer, 1990), as well as the acute bisector (σ_1: maximum shortening direction) for restored conjugate fault populations. Kamb contours were calculated from restored poles to planes using a contour interval of 2σ and a significance level of 1σ. For kinematic data (Fig. 4), FaultKin was used to invert restored minor fault data to model paleostrain axes from eigenvalue statistics on P- and T-axes (Marrett and Allmendinger, 1990). Separate paleostrain analyses are presented that both exclude and include the assumed slip-sense data discussed above. Shortening azimuth results (Table 1) were plotted as a rose diagram to show a mean shortening azimuth from all Zuni minor fault data (Fig. 5).

STRUCTURAL ANALYSIS

Geometric Analysis

Structural data are presented for the northwest and southeast domains and for the range as

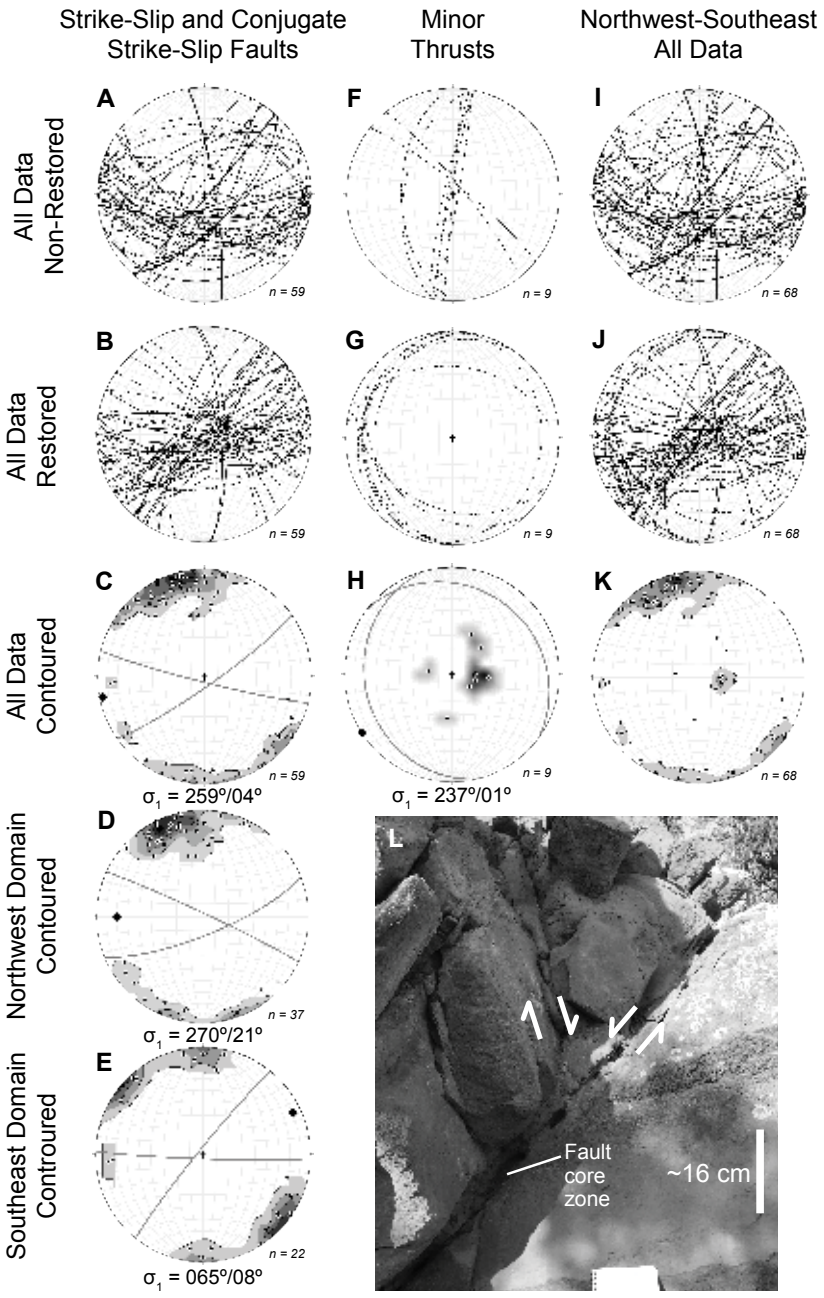


FIGURE 3. Preliminary geometric data and contoured poles to planes on lower hemisphere equal area stereonets. Dashed lines represent northwest domain; solid lines represent southeast domain. **A–E**) Conjugate strike-slip and strike-slip minor fault data. **A**) Non-restored (raw) data. **B**) Data restored to horizontal. **C**) Kamb contoured stereonet, mean planes (gray lines), and acute bisector (black diamond) of all restored conjugate strike-slip and strike-slip minor fault data for the entire Zuni Mountains. **D**) Kamb contoured stereonet, mean planes (gray lines), and acute bisector (black diamond) of restored conjugate strike-slip and strike-slip minor fault data from the northwest domain. **E**) Kamb contoured stereonet, mean planes (gray lines), and acute bisector (black diamond) of restored conjugate strike-slip minor fault data from the southeast domain. **F–H**) Minor thrust-fault data. **F**) Non-restored data. **G**) Restored data. **H**) Kamb contoured stereonet, mean planes (gray lines), and acute bisector (black diamond) of restored minor thrust data points. **I–K**) All data from both domains. **I**) Non-restored data. **J**) Restored data. **K**) Kamb contoured stereonet of all restored data. **L**) Example conjugate fault set used for data collection: looking up at small displacement conjugate fault set in Abo Formation sandstone in the southeast Zuni Mountains.

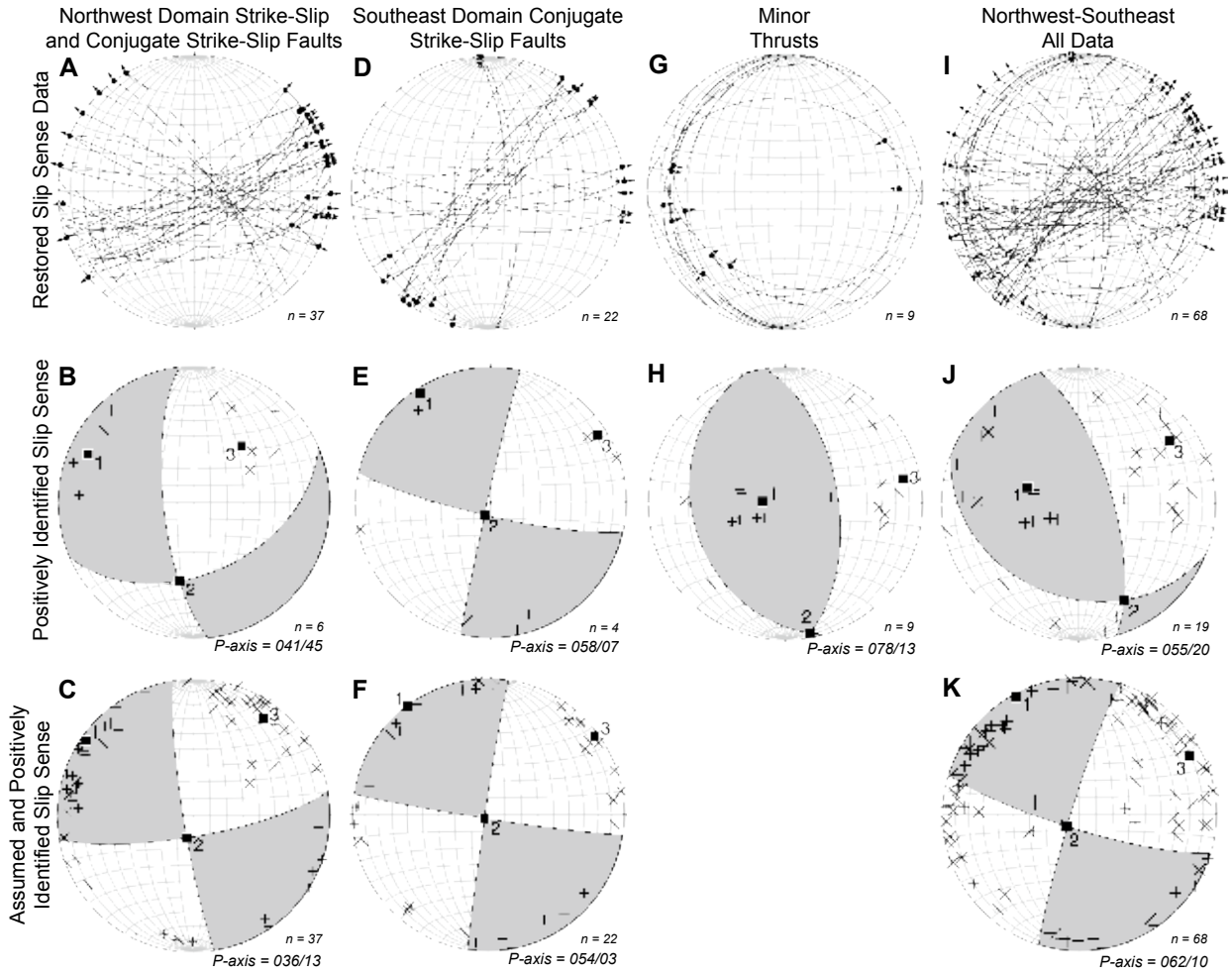


FIGURE 4. Preliminary kinematic data and paleostrain analyses. Arrows show hanging wall slip direction. Crosses (Xs) represent P (compressional) axes; pluses (+s) represent T (dilational) axes. **A–C**) Strike-slip and conjugate strike-slip minor fault data from the northwest domain. **A**) Restored kinematic data. **B**) Paleostrain analysis for only data with positively identified slip sense. **C**) Paleostrain analysis for data with positively identified slip sense and with assumed slip sense. **D–F**) Conjugate strike-slip fault data from the southeast domain. **D**) Restored kinematic data. **E**) Paleostrain analysis for only that data with positively identified slip sense. **F**) Paleostrain analysis for data with positively identified slip sense and with assumed slip sense. **G–H**) Minor thrust data from the northwest domain. **G**) Restored kinematic data. **H**) Paleostrain analysis for minor thrust data (all positively identified slip sense). **I–K**) Data from both domains and for all faults. **I**) Restored kinematic data. **J**) Paleostrain analysis for data with positively identified slip sense. **K**) Paleostrain analysis for data with positively identified slip sense and with assumed slip sense.

a whole in Figure 3 (geometric data) and Figure 4 (kinematic data and paleostrain analyses). All structural data required retrodeformation to a horizontal datum. In all cases, unrestored data displayed an incoherent geometry, whereby restoration to pre-deformation horizontal resulted in coherent fault/fracture geometries (e.g., conjugate), suggesting that these faults formed early in the deformation history prior to considerable strain accumulation (folding and faulting).

The majority of data were collected on strike-slip and conjugate strike-slip minor faults and fractures (Figs. 3A, B). Two dominant pole populations for all strike-slip data are observed that give mean planes of 055°, 83°SE and 104°, 86°S with an acute bisector of trend/plunge (T/P) = 259°/04° (Fig. 3C). Separating conjugate strike-slip faults and fractures into domains produces similar results. Northwest domain strike-slip and conjugate strike-slip minor faults and fractures were collected from Permian and Triassic units within a fault sliver near McGaffey (Figs. 1, 2A). The contoured plot exhibits mean planes of 068°, 76°SE and 295°, 87°NE with an acute bisector of T/P = 270°/21° (Fig. 3D). Southeast domain conjugate strike-slip minor faults and fractures were collected dominantly from the Permian Abo Formation, with mean planes oriented 219°, 86°NW and 092°, 87°S with an acute bisector of T/P = 065°/08° (Fig. 3E).

Minor thrust-fault data (Figs. 3F, G) comprise a small amount of the dataset (n = 9) and were collected only from the northwest domain near McGaffey in the Permian Glorieta Sandstone and Triassic units, as well as at the range front along Forest Service Road 10 within the Cretaceous Gallup Sandstone (Fig. 1). The contoured stereonet results in mean planes oriented 307°, 19°NE and 165°, 20°SW with an acute bisector of T/P = 237°/01° (Fig. 3H).

All data collected for the entire range (Figs. 3I, J) includes strike-slip, conjugate strike-slip, and minor thrust faults. The contoured stereonet in Figure 3K displays seven populations

TABLE 1. Summary table of all shortening azimuths estimated from geometric and kinematic minor fault data (shown in Figs. 3–4). NW: northwest; SE: southeast.

Dataset	Trend	Plunge	Value Type	Analysis Type
All Conjugate Faults (NW and SE Domains) – Fig. 3C	259	04	Acute bisector	Geometric
NW Domain Strike-slip/Conjugate Strike-slip Faults – Fig. 3D	270	21	Acute bisector	Geometric
SE Domain Conjugate Strike-slip Faults – Fig. 3E	065	08	Acute bisector	Geometric
Minor Thrust Faults – Fig. 3H	237	01	Acute bisector	Geometric
NW Domain Strike-slip/Conjugate Strike-slip Faults (Positively Identified Slip Sense) – Fig. 4B	041	45	P-axis (e3*)	Kinematic
NW Domain Strike-slip/Conjugate Strike-slip Faults (With Assumed Data) – Fig. 4C	036	13	P-axis (e3)	Kinematic
SE Domain Conjugate Faults (Positively Identified Slip Sense) – Fig. 4E	058	07	P-axis (e3)	Kinematic
SE Domain Conjugate Faults (With Assumed Data) – Fig. 4F	054	03	P-axis (e3)	Kinematic
Minor Thrust Faults – Fig. 4H	078	13	P-axis (e3)	Kinematic
All Data (Positively Identified Slip Sense) – Fig. 4J	055	20	P-axis (e3)	Kinematic
All Data (With Assumed Data) – Fig. 4K	062	10	P-axis (e3)	Kinematic

* Eigenvector e3 from calculated kinematic P-axes

of poles to planes. These populations are consistent with conjugate fault geometries (two dominant populations with pole populations at north/south and NW/SE), low-angle fault geometries (central population of poles), and high-angle fault geometries (pole populations at west and southwest). A σ_1 estimate is not provided for these data given the variety of fault types.

Kinematic and Paleostrain Analyses

Minor faults with positively identified slip sense comprise ~28% of kinematic data. However, at many locations slip sense could be assumed based on systematic geometries (i.e., conjugate) and/or positively identified slip sense on nearby conjugate faults of similar orientation. Results for data with both positively identified slip sense and assumed slip sense are presented separately for comparison to check the suitability of these assumptions (Fig. 4). In the rotated data in Figure 4, most data with slip lineations along the primitive (outside) circle are assumed with an idealized plunge of 00°.

Strike-slip and conjugate strike-slip minor faults from the northwest domain (Fig. 4A) make up the majority of the currently-available dataset. A paleostrain analysis for positively identified slip-sense data (Fig. 4B) results in a strike-slip fault plane solution with significant oblique slip, and a P-axis oriented T/P = 041°/45°. The paleostrain plot that includes assumed slip-sense data results in a strike-slip fault plane solution with minor oblique slip and a P-axis oriented T/P = 036°/13° (Fig. 4C). Southeast domain conjugate strike-slip minor faults display a clear conjugate geometry (Fig. 4D). Positively identified conjugate strike-slip faults from the southeast domain were collected from bedding with an average orientation of 288°, 50°N, and result in a strike-slip fault plane solution with a P-axis oriented T/P = 058°/07° with minimal oblique slip (Fig. 4E). The southeast domain fault plane solution that includes assumed slip-sense data is strike-slip with a P-axis of T/P = 054°/03° (Fig. 4F). In both the northwest and southeast domains, paleostrain results from positively identified (non-assumed) slip-sense data and assumed slip-sense data produce similar P-axes within 005° azimuth, although appreciable variability in plunge is observed. P-axes compared to acute bisectors from geometric data are markedly different for the northwest domain, although southeast domain P-axis and geometric acute bisector estimates are similar.

Minor thrust-fault data collected from the northwest domain comprises 13% of the overall dataset (Fig. 4G). All kinematic data collected were observed at the outcrop (i.e., no assumed data). Paleostrain analysis results in a thrust-fault plane solution with negligible to very minor oblique slip and a P-axis oriented T/P = 078°/13° (Fig. 4H). The kinematic results show moderate variance with the geometric estimate for shortening (Fig. 3H).

Data from both the northwest and southeast domains include minor strike-slip, conjugate strike-slip, and thrust minor faults (Fig. 4I). Data with positively identified slip sense (Fig. 4J) produce an overall thrust-fault plane solution – given the large amount of thrust-fault data – with marked oblique slip

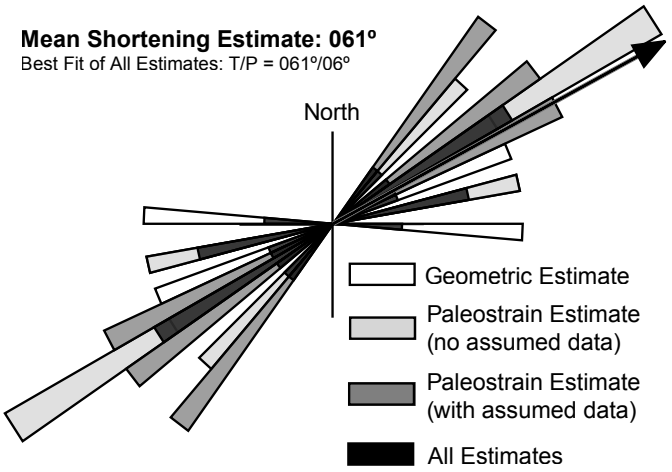


FIGURE 5. Rose diagram showing all shortening azimuths from Table 1 (and text), color-coded by data type. Petals are in 5° increments and scaled to 50% of total perimeter. The mean shortening azimuth (black arrow) is 061°; unique datasets ranged between 051–073° azimuth. A cylindrical best fit of all lineations is trend/plunge (T/P) = 061°/06°.

and a P-axis oriented T/P = 055°/20°. Using both assumed and positively identified slip-sense data produces a strike-slip fault plane solution with minor obliquity (Fig. 4K) – given the large amount of strike-slip fault data – and a P-axis oriented T/P = 062°/10°. Similar P-axis trends are observed for both assumed slip-sense and observed slip-sense data.

DISCUSSION

Laramide Horizontal Shortening and Zuni Arch Formation

Despite opposing reverse-fault polarities between the northwest and southeast domains, preliminary geometric and kinematic data from both parts of the range produce similar results when restored to pre-deformation horizontal. Geometrically, minor strike-slip and conjugate strike-slip faults display ~NE-SW and E-W to ESE-WNW strikes and near-vertical dips (Figs. 3C, D, E). Kinematically, NE-SW and E-W striking planes equate to dextral and sinistral slip, respectively, as shown by paleostrain analyses (Figs. 4B–C, E–F, J–K) that are consistent with field observations. Minor thrust faults show overall N-S and WNW-ESE strikes, although it is important to note the shallow dips of these data (~20°). Given the shallow dip, minor thrust data may actually represent Riedel R or P minor faults rather than true thrust faults, although similarly shallow conjugate thrust faults have been documented in other Laramide deformation studies (e.g., Singleton et al., 2019). Kinematic analysis of minor thrust data shows NNW-SSE striking dip slip low- and moderate-angle nodal planes (Fig. 4H). Continued data collection will produce a more robust mean estimate for all faults, especially minor thrust faults, and will give preference to minor faults that exhibit shear sense criteria. Overall, it is notable that minor fault geometries are similar between the northwest and southeast domains and for the range as a whole.

Shortening directions are geometrically estimated from the acute bisector ($\sigma 1$) of conjugate strike-slip minor faults in all geometric data (Fig. 3) and kinematically estimated from P-axes utilizing both positively identified slip-sense data and assumed slip-sense data (Fig. 4). Shortening azimuths from both geometric and kinematic datasets show similar results, as synthesized in Table 1. A rose diagram of all geometric and kinematic shortening estimates (Fig. 5) produces a mean shortening azimuth of 061°. A cylindrical best fit to all shortening lineation estimates is T/P = 061°/06°. The mean shortening estimate for each data type ranges between 051–073° azimuth. Collection of these data from NNE-SSW, N-S, NNW-SSE, and ENE-WSW striking beds shows that the shortening estimate does not reflect preferential sampling and further suggests that results record early horizontal shortening that preceded significant strain accumulation (i.e., formed prior to significant folding and faulting). Continued data collection will likely diminish the spread shown by the Figure 5 rose diagram. However, the shortening azimuth provided here from preliminary data is consistent with early suggestions of 060° shortening for the southern San Juan Basin and Zuni arch (Smith, 1957).

WSW-ENE shortening has been documented on a variety of Laramide structures throughout the Colorado Plateau and Rocky Mountain regions from Montana–South Dakota to northern Arizona–New Mexico (Bump and Davis, 2003; Bump, 2004; Erslev and Koenig, 2009; Weil and Yonkee, 2012; Singleton et al., 2019). It is interesting to note the remarkable similarity in average shortening azimuths across the entire expanse of the Laramide foreland region as exemplified by an array of researchers, methods, and datasets, although some variability has been mentioned (e.g., ~N-S shortening: Craddock and van der Pluijm, 1999). This is especially true when comparing the results herein with shortening estimates from the most distal Laramide arch, the Black Hills in South Dakota–Wyoming, and its documented mean shortening azimuth of ~068° (Singleton et al., 2019). Similar Late Cretaceous–Paleogene mean shortening directions for numerous Laramide arches suggests (1) a consistent regional shortening direction for the entire Laramide foreland and (2) that Laramide structures, although variably oriented, likely formed from pervasive WSW-ENE-directed shortening. Perseverance of this shortening direction across the Colorado Plateau and Rocky Mountain regions also, by extrapolation, suggests similar formational processes for Laramide structures in both of these distinct provinces, despite marked structural differences (namely less accumulated strain on Colorado Plateau structures).

Other mechanisms cited for formation of the Zuni arch are less attractive in light of a regionally consistent shortening direction and observation of early horizontal shortening. The structural complexity called upon by Chamberlin and Anderson (1989, Fig. 3) as evidence for Eurasian style extrusion tectonics is more likely attributable to variable reactivation of older faults from Proterozoic extension and/or contractional orogenesis related to the Ancestral Rocky Mountains. Reactivation would have been within a simple WSW-ENE shortening direction. Furthermore, similar fault geometries and shortening estimates from both ends of the range are not consistent

with westward extrusion of the northwest Zuni Mountains, as different shortening estimates would be expected for each part of the range (e.g., west-oriented P-axes in the northwest and north- to northeast-oriented P-axes in the southeast). However, this does not negate the role that the interpreted mafic crustal anomaly (Chamberlin and Anderson, 1989) may have played on localizing upper crustal strain here. Preliminary results do, however, negate early vertical uplift followed by later horizontal shortening (Anderson et al., 2003). Early horizontal shortening was likely established prior to significant folding and faulting, as clear fault geometries are noted when data is restored to pre-deformation horizontal (Figs. 3B, G, J).

Hypothesized Role of Sinistral Faulting Within the Laramide Zuni Arch

East-striking faults mapped by Goddard (1966) at scale 1:31,680 and Hackman and Olson (1977) at scale 1:250,000 are coincident with the central portion of the range. Taking into consideration the kinematic results (Fig. 4) and WSW-ENE directed shortening (Fig. 5), east-striking faults in the Zuni arch would have been susceptible to sinistral slip during Laramide contraction. Sinistral slip between two oppositely directed reverse faults in the northwest (southwest-directed) and southeast (northeast-directed) domains is kinematically feasible, and would suggest that the central Zuni arch deformed via sinistral displacement transfer as strain from the northwest transferred to the southeast (or vice versa). Such kinematics have been suggested for the Laramide Beartooth arch in southwest Montana by impingement of the shallow crustal ultramafic-mafic Stillwater Complex along its north-central margin (Wise, 2000). Similar to the Zuni range, the northwest Beartooth arch is characterized by southwest-directed folds and faults (near Gardiner, Montana), while northeast-directed folds and faults characterize the southeast Beartooth arch (e.g., Red Lodge, Montana). Both ends are connected by a discrete structure, the Mill Creek-Stillwater fault zone, which may have localized sinistral displacement transfer. The similar structural framework and the possible role of mafic "indenters" (Stillwater Complex and El Morro Gravity High of Chamberlin and Anderson, 1989) suggest a potential commonality between Zuni and Beartooth arch formation whereby crustal heterogeneity may have localized and/or deflected upper crustal strain.

However, kinematic evidence in support of sinistral displacement transfer for the central domain is thus far lacking. The major easterly striking fault in the central portion of the Zuni Mountains (Fig. 1) was originally mapped by Goddard (1966) as a fault zone with silicified breccia and slickensided planes of 40° oblique dextral slip. This "fault" is actually a (Proterozoic?) pegmatite dike with no associated breccia zones or fault surfaces, based on field examination of this feature in the summer of 2019. More east to east-southeasterly striking faults are mapped by Goddard (1966) as sinistral within the central domain and in the southeast domain near New Mexico State Route 53. Additionally, Chamberlin and Anderson (1989) suggest that numerous easterly striking faults are sinistral on their Zuni Mountains tectonic map. Furthermore, northerly striking dextral faults (including the Sedgwick reverse fault) are kinematically viable considering the results presented in this study (e.g., Fig. 4K). Given these mapped structures and the preliminary results of this work, future studies will focus on easterly striking structures in the Zuni arch, especially within the central domain, to test the hypothesis of sinistral displacement transfer.

FUTURE WORK

The preliminary work presented here outlines a structural framework for the Zuni arch that can be expanded upon by future studies. Of first order importance is the accumulation of a larger and more comprehensive structural dataset that will better characterize fault geometries and kinematics and produce a robust estimate of Late Cretaceous–Paleogene shortening for the range. Secondly, the character of deformation and its kinematics in the central domain are of utmost interest for deciphering how strain transferred between the NE-dipping Stinking Springs and McGaffey reverse faults and the SW-dipping Sedgwick reverse fault. Inherently and in accord, distinct intra-range structural complexities are in need of attention to better understand both Laramide and Ancestral Rocky Mountains deformation.

The southeast Zuni Mountains highlight a key question: what is the role of the southwest dipping Sedgwick reverse fault? The pervasive dip of the Chaco Slope deep into the San Juan basin (e.g., Cather, 2004) would suggest that the controlling structure for the Zuni arch is a NE-dipping reverse/thrust fault. Therefore, it is possible that the Sedgwick reverse fault was a backthrust off a main thrust at depth (the "Zuni thrust"). Particularly interesting is the observation that the northwest Zuni Mountains are relatively more shortened, via the Nutria monocline bounding the Gallup sag, but are lower topographically, while the southeast Zuni Mountains are less shortened but more uplifted via the Sedgwick reverse fault, as shown by the expansive basement outcrop in the southeast and the topographic highpoint of Mt. Sedgwick. Assuming a northeast-dipping master thrust, a backthrusted Sedgwick reverse fault would have exploited an initially high structural level that then, through progressive deformation, produced a structurally higher although minimally deformed block via the Sedgwick reverse fault. Alternatively, the observed disparity could be related to warping related to the elevated temperatures along the Jemez lineament. These hypotheses can be tested through cross-section balancing and forward kinematic modeling.

CONCLUSIONS

Characteristic minor fault geometries and kinematics are documented in the Zuni arch that include NE-SW and E-W striking strike-slip and conjugate strike-slip faults and N-S to NNW-SSE striking reverse and thrust faults. Horizontal shortening was established early in the deformation history prior to significant folding and faulting. Fault geometries and kinematics are similar for both the northwest and southeast Zuni Mountains, despite marked differences in the structural style at both ends of the range. Geometric and kinematic analyses produce a

WSW-ENE-directed shortening estimate (061° mean azimuth) that is attributed to reflect the orientation of horizontal shortening responsible for formation of the Zuni arch, and is consistent with most shortening estimates from numerous Colorado Plateau and Rocky Mountain Laramide arches. Therefore, it seems likely that Laramide arches throughout the entire interior western U.S.A. formed from similar tectonic processes, and not from special and localized mechanisms that have been previously proposed for the Zuni arch (extrusion tectonics and vertical uplift). The structural framework and shortening azimuth may have been conducive for a zone of sinistral displacement transfer within the central part of the arch during Laramide deformation. Future work will address this hypothesis, as well as other aspects of the range's structural complexity.

ACKNOWLEDGMENTS

A portion of a UNM GPSA grant supported a portion of the fieldwork costs. This paper benefited from reviews by Dr. Jason Ricketts (UTEP), Dr. Steve Cather (NMBGMR), and Dr. Karl Karlstrom (UNM), and by the editors Drs. Shari Kelley and Kate Zeigler. Dan Young, Katie Holleron, and Shoshone-Nizhoni (Shoni) Dog were of great help in the field.

REFERENCES

Allmendinger, R.W., Cardozo, N., and Fisher, D.M., 2012, Structural Geology Algorithms: Vectors and Tensors: Cambridge, Cambridge University Press, 302 p.

Anderson, O.J., Maxwell, C.H., and Lucas, S.G., 2003, Geology of Fort Wingate quadrangle, McKinley County, New Mexico: New Mexico Bureau of Geology and Mineral Resources Open-File Report 473, scale 1:24,000, 15 p.

Bump, A.P., 2004, Three-dimensional Laramide deformation of the Colorado Plateau: Competing stresses from the Sevier thrust belt and the flat Farallon slab: Tectonics, v. 23, https://agupubs.onlinelibrary.wiley.com/doi/10.1029/2002TC001424.

Bump, A.P., and Davis, G.H., 2003, Late Cretaceous–early Tertiary Laramide deformation of the northern Colorado Plateau, Utah and Colorado: Journal of Structural Geology, v. 25, p. 421–440.

Cardozo, N., and Allmendinger, R.W., 2013, Spherical projections with OSX-Stereonet: Computers & Geosciences, v. 51, p. 193–205.

Cather, S.M., 1990, Stress and volcanism in the northern Mogollon-Datil volcanic field, New Mexico: Effects of the post-Laramide tectonic transition: Geological Society of America Bulletin, v. 102, p. 1447–1458.

Cather, S.M., 2004, Laramide orogeny in central and northern New Mexico and southern Colorado, *in* Mack, G.H., and Giles, K.A., eds., The Geology of New Mexico, A Geologic History: New Mexico Geological Society Special Publication 11, p. 203–248.

Chamberlin, R.M., and Anderson, O.J., 1989, The Laramide Zuni uplift, southeastern Colorado Plateau: A microcosm of Eurasian-style indentation-extrusion tectonics?: New Mexico Geological Society, Guidebook 40, p. 81–90.

Coney, P.J., and Reynolds, S.J., 1977, Cordilleran Benioff zones: Nature, v. 270, p. 641–644.

Craddock, J.P., and van der Pluijm, B.A., 1999, Sevier–Laramide deformation of the continental interior from calcite twinning analysis, west-central North America: Tectonophysics, v. 305, p. 275-286.

Darton, N.H., 1928, "Red beds" and associated formation in New Mexico, with an outline of the geology of the state: U.S. Geological Survey, Bulletin 794, no. 3, 298 p.

Dickinson, W., and Snyder, W.S., 1978, Plate tectonics of the Laramide orogeny: Geological Society of America, Memoir 151, p. 355-366.

Edmonds, J.R., 1961, Geology of the Nutria monocline, McKinley County, New Mexico [M.S. thesis]: Albuquerque, University of New Mexico, 100 p.

Erslev, E.A., and Koenig, N.V., 2009, Three-dimensional kinematics of Laramide, basement-involved Rocky Mountain deformation, USA: Insights from minor faults and GIS-enhanced structure maps, *in* Kay, S.M., Ramos, V.A., and Dickinson, W.R., eds., Backbone of the Americas: Shallow Subduction, Plateau Uplift, and Ridge and Terrane Collision: Geological Society of America, Memoir 204, p. 125–150.

Goddard, E.N., 1966, Geologic map and sections of the Zuni Mountains fluorspar district, Valencia County, New Mexico: U.S. Geological Survey, Miscellaneous Investigations Map I-454, scale 1:31,680.

Green, G.N. and Jones, G.E., 1997, The digital geologic map of New Mexico in ARC/INFO format: U.S. Geological Survey Open-File Report 97-0052, 9 p.

Hackman, R.H., and Olson, A.B., 1977, Geology, structure, and uranium deposits of the Gallup 1 degree x 2 degree quadrangle, New Mexico and Arizona: Washington, D.C., U.S. Geological Survey, Miscellaneous Investigations Series I-981, scale 1:250,000, 2 sheets.

Kelley, V.C., 1967, Tectonics of the Zuni-Defiance region, New Mexico and Arizona: New Mexico Geological Society, Guidebook 18, p. 28–31.

Marrett, R.A., and Allmendinger, R.W., 1990, Kinematic analysis of fault-slip data: Journal of Structural Geology, v. 12, p. 973–986.

Petit, J.P., 1987, Criteria for the sense of movement on fault surfaces in brittle rocks: Journal of Structural Geology, v. 9, p. 597–608.

Ross, C.A., and Ross, J.R.P., 1986, Paleozoic paleotectonics and sedimentation in Arizona and New Mexico, *in* Peterson, J.A., ed., Paleotectonics and Sedimentation in the Rocky Mountain Region, United States: Tulsa, American Association of Petroleum Geologists, Memoir 41, p. 653–668.

Singleton, J.S., Mavor, S.P., Seymour, N.M., Williams, S.A., Patton, A.I., Ruthven, R.C., Johnson, E.P., and Prior, M.G., 2019, Laramide shortening and influence of Precambrian basement on uplift of the Black Hills, South Dakota and Wyoming, U.S.A.: Rocky Mountain Geology, v. 54, p. 1–17.

Smith, C.T., 1957, Geology of the Zuni Mountains, Valencia and McKinley Counties, New Mexico: Four Corners Geological Society, Guidebook, p. 53–61.

Strickland, D., Heizler, M.T., Selverstone, J., and Karlstrom, K.E., 2003, Proterozoic evolution of the Zuni Mountains, western New Mexico: Relationship to the Jemez lineament and implications for a complex cooling history: New Mexico Geological Society, Guidebook 54, p. 109–117.

Timmons, J.M., and Cikoski, C.T., 2012, Geologic map of the San Rafael quadrangle, Cibola County, New Mexico: New Mexico Bureau of Geology and Mineral Resources, Open-file Geologic Map 232, scale 1:24,000.

Vollmer, F.W., 1990, An application of eigenvalue methods to structural domain analysis: Geological Society of America Bulletin, v. 102, p. 786–791.

Weil, A.B., and Yonkee, W.A., 2012, Layer-parallel shortening across the Sevier fold-thrust belt and Laramide foreland of Wyoming: Spatial and temporal evolution of a complex geodynamic system: Earth and Planetary Science Letters, v. 357–358, p. 405–420.

Wise, D.U., 2000, Laramide structures in basement and cover of the Beartooth Uplift near Red Lodge, Montana: American Association of Petroleum Geologists Bulletin, v. 84, p. 360–375.

Worthington, L.L., Miller, K.C., Erslev, E.A., Anderson, M.L., Chamberlain, K.R., Sheehan, A.F., Yeck, W.L., Harder, S.H., and Siddoway, C.S., 2016, Crustal structure of the Bighorn Mountains region: Precambrian influence on Laramide shortening and uplift in north-central Wyoming: Tectonics, v. 35, p. 208–236.